SOL ENGINEERING SERVICES

Limits of Conventional Liquid Cold Plates and Jet-Impingement Crossflow

Performance ceilings of machined and brazed cold plates, crossflow degradation in jet arrays, return-port architectures and mass scaling

Prepared for DEVCOM Army Research Laboratory, the Ground Vehicle Systems Center, and university and industry partners of the CF-JET effort

Classification	Unclassified. Prepared from open-source information.
Date	23 November 2026

Executive Summary

Conventional single-phase liquid cold plates reach a floor near 100 to 200 mm²·K/W in the finned and swaged-tube forms, and published microchannel, pin-fin and jet results fall between 9 and 158 mm²·K/W once each is divided by the area on which it was measured (Table 2). The CF-JET design point of 1.5 kW on a 60 mm by 60 mm footprint with a case-to-coolant resistance target of 0.02 K/W converts to 72 mm²·K/W (derived).[1] That value is 1.4 times better than the finned cold plate figure in patent background and 2.8 times better than the swaged-tube figure.[2] It allows 3.6 times the resistance of the jet-impingement convective values that the National Renewable Energy Laboratory (NREL) reports.[3] The target is aggressive against conventional cold plates and lies inside the range that published jet and microchannel results have reached.

Six findings support that conclusion.

- **Conventional ceilings.** Patent background places the floor of a swaged-tube cold plate at about 2 K·cm²/W and a finned cold plate at about 1 K·cm²/W.[4] Additively manufactured and machined single-phase plates reported in peer-reviewed work reach 31 to 94 mm²·K/W (derived) on areas of 1.4 to 6.5 cm² (Table 2).[5][6]
- **Jet heat transfer.** Jets give the highest local coefficients, up to three times those of confined channel flow at the same maximum velocity in a review by Zuckerman and Lior.[7] The area-averaged coefficient is much lower than the local value: a numerical study at Oak Ridge National Laboratory reports 210 kW/m²·K locally and 6.34 kW/m²·K averaged over the substrate.[8] Single-phase microchannels and microtubes have reached 790 and about 3,000 W/cm², and a hybrid microchannel and slot-jet module reached 305.9 W/cm² without phase change.[9][10]
- **Crossflow.** Spent fluid from upstream jets reduces downstream heat transfer. The Florschuetz correlation, developed with air, predicts that a jet row preceded by ten upstream rows at x/d = 8, y/d = 6 and z/d = 2 retains 65 percent of its crossflow-free Nusselt number in an in-line array and 55 percent in a staggered array (derived, Table 4).[11]
- **Return ports.** Simulations with interspersed extraction ports report lower average temperatures, better uniformity and modest pressure drops, and experiments with spent-air exits report higher coefficients (Table 5).[12][13] Manifold losses account for a large share of the pressure drop in the 3D-printed water device that was tested.[14]
- **Mass.** Copper has 3.3 times the density of aluminum. A 60 mm by 60 mm by 3 mm plate has a mass of 96 g in copper and 29 g in aluminum (derived). An additively manufactured aluminum alloy has a thermal conductivity per unit density 17 percent higher than that of copper (derived, Table 6). In an NREL cold plate study, a glass-fiber reinforced nylon construction saved about half of the assembly mass, which indicates that construction choices outside the conduction path account for a large share of the mass.[15]
- **Evidence limits.** The Florschuetz correlation was fitted to air. No public source found links cold plate mass to thermal resistance for vehicle or aerospace use. Several benchmark results are numerical and are labeled in Table 2.

The paper recommends that the CF-JET effort define the reference plane of the case temperature, report resistance per unit area and conductance per unit mass alongside pressure drop, set the return-port spacing so that the crossflow ratio stays at or below about 0.3, and measure crossflow degradation on a representative sub-array with the 50/50 water-glycol coolant.

1. Introduction and Scope

A liquid cold plate removes heat from a power module through a conduction path and a convective path, and each path has a ceiling. This paper describes where those ceilings lie for machined and brazed aluminum and copper cold plates, how jet impingement changes the convective ceiling, why crossflow limits jet arrays, and how mass scales with performance. The intended readers are program managers at the U.S. Army DEVCOM Army Research Laboratory, engineers at the Ground Vehicle Systems Center (GVSC), university co-investigators and industry partners.

Four questions organize the paper. What thermal resistance and heat transfer coefficients do state-of-the-art microchannel, pin-fin and jet-impingement cold plates achieve? How does crossflow from upstream jets degrade downstream heat transfer, and which correlations capture it? Which return-port and manifold architectures reduce crossflow? How does cold plate mass scale with performance? Table 1 states three claims that the paper tests and gives the verdicts.

Table 1. Three claims tested and the verdicts

Claim	Verdict	Basis for the verdict
Copper has a density of about 8.9 g/cm³ and aluminum about 2.7 g/cm³.	Supported	The Copper Development Association gives 8.89 g/cm³ as the standard value and 8.92 g/cm³ as typical at 20 °C. A peer-reviewed study of 3D-printed cold plates lists 8.89 g/cm³ for a copper alloy and 2.7 g/cm³ for the aluminum alloy AlSi10Mg.[16][17]
Jet impingement is among the highest single-phase liquid heat transfer methods.	Supported for local coefficients; qualified for area-averaged coefficients and for heat flux	Local coefficients of 210 to 250 kW/m²·K are reported for jets. The area-averaged value in one numerical study is 6.34 kW/m²·K, and single-phase microchannels and microtubes have reached 790 to about 3,000 W/cm².[18][19][20][21]
A case-to-coolant resistance of 0.02 K/W or less at 1.5 kW is aggressive yet achievable.	Supported, conditional on the definition of the case reference plane	The target equals 72 mm²·K/W on the footprint. It is better than the conventional cold plate floors and allows 1.0 to 8 times the resistance of published jet and microchannel results (Table 7).[22][23]

Verdicts apply to the sources reviewed. Table 7 compares the target with published results.

The CF-JET effort, proposed by SOL Engineering Services, LLC, applies an additively manufactured, liquid-cooled jet-impingement cold plate with interleaved return ports and an optimized carbon fiber target plate to the thermal management of power modules.[24] The representative design point used in this paper is 1.5 kW on a 60 mm by 60 mm footprint, 50/50 water-glycol coolant at 65 °C inlet, a flow of 4 to 8 L/min and a pressure drop of 30 kPa or less. These values come from the proposal and are design assumptions. The paper tests them against the published record and states the open questions. Figure 1 shows the heat path and the resistance budget.

Figure 1. Heat path and resistance budget of a liquid-cooled cold plate

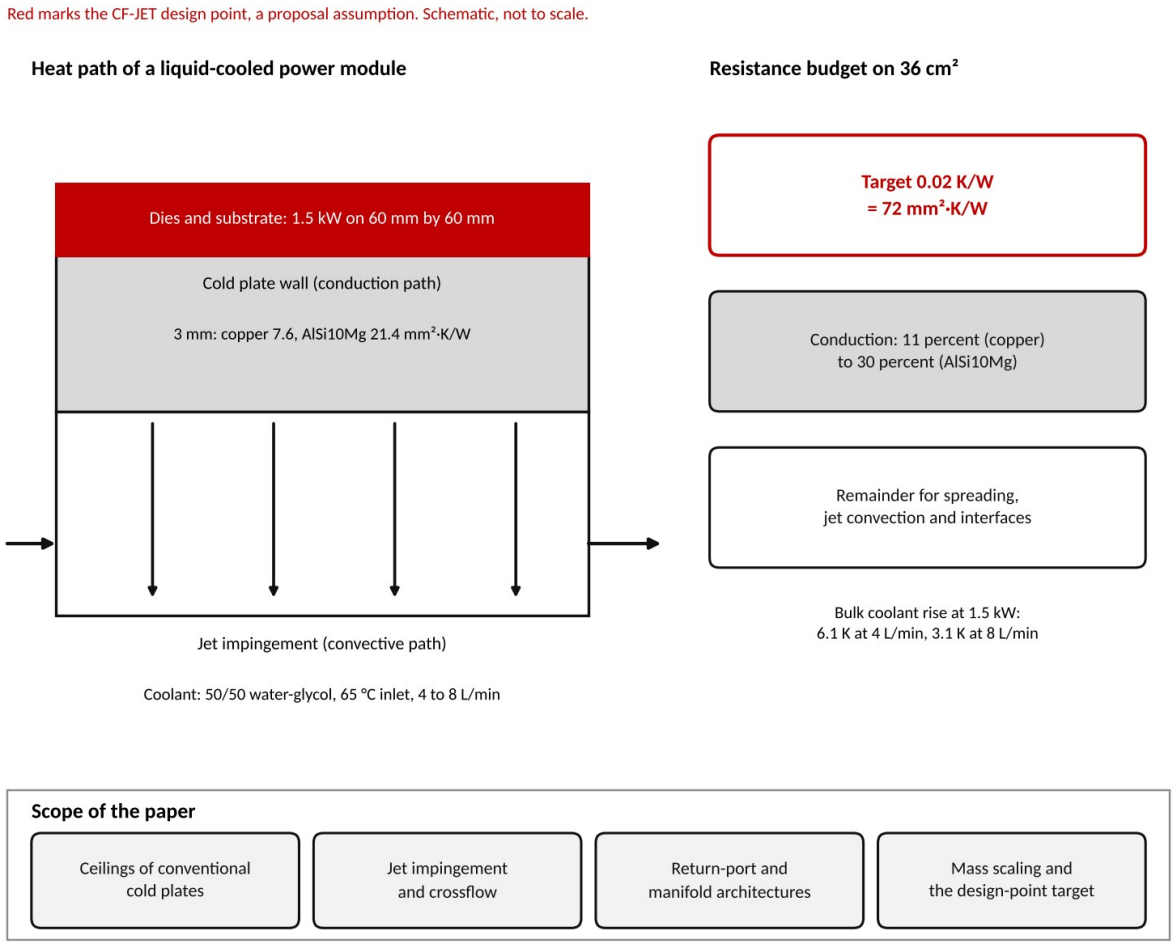

The 72 mm²·K/W target, the flow and the coolant are proposal assumptions.[25] *Conduction values and the coolant rise are derived in this paper. The diagram is schematic and not to scale.*

2. Performance Ceilings of Conventional Cold Plates

2.1 Swaged-tube and finned cold plates have a floor near 100 to 200 mm²·K/W

The background section of a microchannel patent states that a conventional swaged-tube cold plate reaches a minimum thermal resistance of about 2 °C per W/cm² and that finned cold plates reach about 1 °C per W/cm².[26] The units convert directly: 2 K·cm²/W equals 200 mm²·K/W, and 1 K·cm²/W equals 100 mm²·K/W. The patent is a manufacturer's document that promotes microchannel heat exchangers, and the figures are approximate statements of practice. No test conditions accompany them. They remain useful as a stated reference for machined and brazed construction because they use the same area-normalized form that the other benchmarks in this paper use.

Area normalization multiplies a measured resistance in K/W by the heated area. The product has units of K·cm²/W and allows plates of different sizes to be compared. A plate with a stated resistance of 0.05 K/W on 6.5 cm² and a plate with 0.5 K/W on 0.65 cm² have the same normalized value of 0.32 K·cm²/W (32 mm²·K/W).

2.2 Microchannel, pin-fin and manifold designs reach 30 to 95 mm²·K/W when normalized by area

Table 2 lists the benchmarks found in the sources reviewed, with each resistance converted to mm²·K/W on the area stated in the source. Figure 2 plots the converted values against the CF-JET target. The silicon microchannel heat sink of Tuckerman and Pease removed 790 W/cm² at a 71 K temperature rise on a 1 cm² chip, which corresponds to about 0.09 K/W and 9 mm²·K/W.[27] The best additively manufactured plates reported in peer-reviewed work are within a factor of about 3 to 10 of that result.

Table 2. Reported cold plate and jet-impingement results, converted to area-normalized resistance

Design	Source and basis	Reported result	Area (cm²)	Resistance (mm²·K/W, derived)
Swaged-tube cold plate	Patent background[28]	Minimum about 2 K·cm²/W	Per unit area	200
Finned cold plate	Patent background	About 1 K·cm²/W	Per unit area	100
Single-phase silicon microchannel	Tuckerman and Pease, 1981, measured	790 W/cm² at 71 K rise; about 0.09 K/W	1	9
Straight microchannel, AlSi10Mg	Collins et al., 2019, measured	0.29 to 0.50 K/W over 500 to 2,000 kg/m²·s	1.44	42 to 72
Manifold microchannel, AlSi10Mg	Collins et al., 2019, measured	0.45 to 0.65 K/W	1.44	65 to 94
Impingement pin-fin cold plate, AlSi10Mg	Hoang et al., 2022[29]	0.064 to 0.067 K/W at 2 L/min; 21.1 to 28.1 kPa	6.45	41 to 43
Impingement pin-fin cold plate, copper alloy	Hoang et al., 2022, material comparison (numerical)	0.048 K/W at 1 L/min; 8.14 kPa	6.45	31
Hotspot micro pin fins	Fallahtafti et al., 2022 (numerical)[30]	0.208 K·cm²/W at about 10 kPa	Per unit area	21
Jet array on AlSiC plate	Pahinkar et al. (numerical)[31]	57 kW/m²·K at 40 kPa and 0.094 kg/s	Per unit area	17.5
Jet impingement, convective path	NREL annual report[32]	Below 20 mm²·K/W	Per unit area	Below 20
SiC half-bridge module with jets	NREL, 2025, measured[33]	Junction-to-fluid as low as about 15 mm²·K/W	Not stated	About 15
Jet substrate cooling	Barua et al., 2022 (numerical)[34]	Area-averaged 6.34 kW/m²·K	Per unit area	158
CF-JET target	SOL proposal[35]	0.02 K/W at 1.5 kW	36	72

Resistance in mm²·K/W is the reported K/W multiplied by the stated area, or the reciprocal of the reported coefficient. Areas are the heater or fin areas given in each source. Hoang et al. state a 25.4 mm square fin area. The NREL half-bridge value is junction-to-fluid and includes the module stack. Sources are peer-reviewed except the patent background, the NREL report and the draft conference paper.

Figure 2. Area-normalized resistance of reported cold plate and jet-impingement results against the CF-JET target

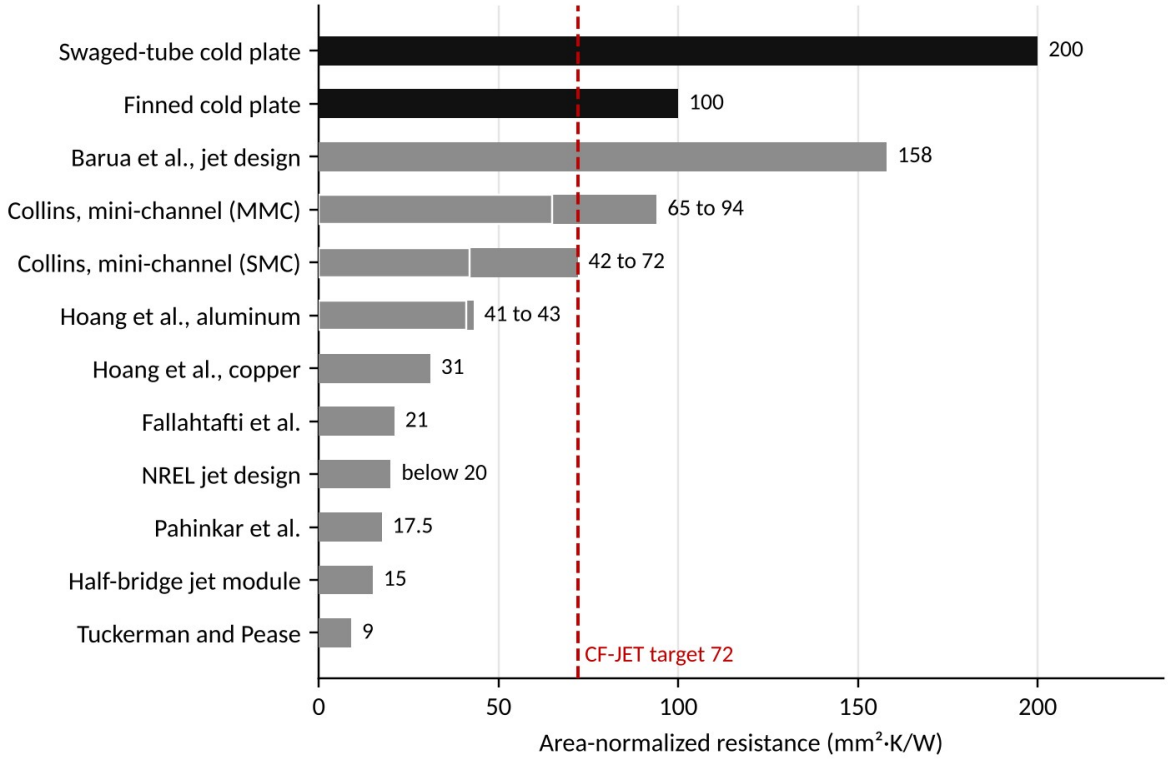

Black bars are reported resistances multiplied by the stated area. Grey bars are derived from reported coefficients or from numerical results. The red dashed line is the CF-JET target of 72 mm²·K/W. All bar values are derived in this paper from the cited sources.

Two features of Table 2 affect how the values are read. The areas differ by a factor of 36 across the table, and the smallest areas favor the lowest normalized values because the heat flux per unit footprint is high and the spreading path is short. The measured values also include different parts of the thermal path. Tuckerman and Pease report a chip-to-coolant rise, Collins et al. report a rise from the heater to the inlet water, and the NREL half-bridge value spans the module stack to the fluid. The comparison with the target therefore has an uncertainty that the definition of the case reference plane settles (Table 7).

2.3 Additive manufacturing limits the conductivity and surface of the plate

Additively manufactured aluminum plates have a lower conductivity and a rougher surface than wrought metal. Collins et al. built straight and manifold microchannel heat sinks in AlSi10Mg by direct metal laser sintering with 500 µm hydraulic diameters and measured a surface roughness (Ra) of about 20 µm, a conductivity of 110 W/m·K and turbulence onset at Reynolds numbers of 600 to 800.[36] Hoang et al. list 140 W/m·K for AlSi10Mg and 380.2 W/m·K for a copper alloy in their material comparison.[37] The two aluminum figures differ by 27 percent, which indicates the range that process and heat treatment produce. For a CF-JET body printed in metal, the conductivity of the printed material governs the spreading resistance and has to be measured on the finished part.

The manifold microchannel in the same study cut the pressure drop by about 90 percent at a Reynolds number near 210 and by 40 percent near 1,175, and its thermal resistance was higher than that of the straight microchannel at every tested flow (0.45 to 0.65 K/W against 0.29 to 0.50 K/W).[38] The result shows the trade that return and manifold architectures impose: a lower pressure drop and a higher resistance for the same footprint.

2.4 The coefficient that the target requires depends on the conduction share

The 72 mm²·K/W target divides among conduction through the plate, spreading and convection, and the share left for convection fixes the coefficient that the jets must deliver. If convection takes the whole budget, the footprint-averaged coefficient must be 13.9 kW/m²·K. If conduction and spreading take 25 percent of the budget (18 mm²·K/W), convection has 54 mm²·K/W and the coefficient rises to 18.5 kW/m²·K. If they take 50 percent, the coefficient is 27.8 kW/m²·K.[39] A 3 mm AlSi10Mg plate alone consumes 21.4 mm²·K/W in one-dimensional conduction (Table 6), which is 30 percent of the budget.

The published jet results span this requirement. The jet array of Pahinkar et al. corresponds to 57 kW/m²·K in a numerical study, and the Oak Ridge jet design averages 6.34 kW/m²·K over its substrate in another numerical study.[4041] The required coefficient lies between those two values, so the verdict on the target depends on which of them the CF-JET geometry resembles.

Three features of the CF-JET concept bear on that comparison. The carbon fiber target plate conducts heat from the die footprint through perpendicular fibers, which reduces the conduction term relative to a solid aluminum plate of equal thickness if the fiber conductivity along the fiber axis is high. The thin electroplated metal face limits the added conduction path and seals the fiber ends against coolant. The interleaved return ports limit the crossflow that degrades the coefficient in long arrays. Each feature is a SOL proposal assumption. No independent result reviewed measures a carbon fiber insert target under a jet array, so the effect of the first feature on the conduction term is an open measurement.[42]

3. Jet-Impingement Heat Transfer

3.1 Jets deliver the highest local coefficients

Zuckerman and Lior review the physics and correlations of jet impingement and state that jets can give coefficients up to three times those of confined wall-parallel flow at the same maximum flow speed.[43] For an isolated round jet at H/D = 6 and a Prandtl number of 0.7, they tabulate Nusselt numbers of about 19 at Re = 2,000 and about 212 at Re = 100,000.[44] Walsh reports a heat transfer coefficient of about 250 kW/m²·K for an array of sixteen 100 µm jets in a thesis at the Massachusetts Institute of Technology, and the heat flux basis of that value is not restated here.[45] Barua et al. calculate a local jet coefficient of about 210 kW/m²·K for a SiC substrate cooling design.[46] These local results support the claim that jets rank among the highest single-phase liquid heat transfer methods at the point of impingement.

3.2 The area-averaged coefficient is far below the local value

The same Oak Ridge study reports an area-averaged coefficient of 6.34 kW/m²·K for the jet design against local values near 210 kW/m²·K, a ratio of about 33 (derived), and reports 30 kW/m²·K for a pin-fin heat sink and 100 kW/m²·K for a genetic-algorithm optimized heat sink.[47] The study is a numerical comparison, and the area basis of each value is that of the source. The gap is consistent with a stagnation region that covers a small fraction of the target surface. The convective resistance of a cold plate depends on the area average. A design that cites the local coefficient overstates the performance.

Zuckerman and Lior note that jet interaction is significant at a jet pitch-to-diameter ratio below 4 and a minor factor at pitch-to-diameter ratios of 8 and above with H/D of 2 or more.[48] Small pitches raise the coefficient density and increase the interaction between neighboring wall jets. Large pitches reduce the interaction and lower the number of stagnation regions per unit area.

3.3 Measured gains of jets over channel flow in power electronics are 12 to 44 percent in resistance

NREL compared a commercial channel-flow inverter heat exchanger with jet impingement on plain and microfinned surfaces. In dynamometer tests at 40 to 100 kW output power, the junction-to-coolant resistance fell by up to 12.5 percent, the baseplate-to-coolant (convective) resistance fell by up to 37.0 percent and the coefficient of performance improved by up to 13 percent for jets on enhanced surfaces.[49] The presentation abstract states that with jet impingement the cold plate material matters little for the thermal path, a result that bears on the choice of material for CF-JET.[50]

A modeled NREL design case at 2.5 kW, 10 L/min and 50/50 water-ethylene glycol at 70 °C gives a junction-to-ambient resistance of 0.294 K/W for channel flow, 0.191 K/W for jets on a plain surface (34 percent lower) and 0.166 K/W for jets on a microfinned surface (44 percent lower). The pressure drop was 16,858 Pa for channel flow and 17,458 Pa for both jet designs, which is 600 Pa or 3.6 percent more than channel flow (derived).[51] A small pressure penalty paired with a resistance reduction of 34 to 44 percent at the same 10 L/min is the performance case for jets over channels that the sources support, and it is a modeled result. The page reports that the 180-day reliability test left the nozzle diameter unchanged and produced oxidation, and that CFD gives up to 79 percent higher power density and 118 percent higher specific power. The measured and modeled gains in resistance, 12.5 to 44 percent, are smaller than the factor of up to three in the coefficient, which is consistent with the convective path being one part of the total resistance.

4. Crossflow Degradation in Jet Arrays

4.1 Spent fluid from upstream jets accumulates and deflects downstream jets

In an array that drains toward one side, the spent fluid of every jet crosses the jets that lie downstream, and the crossflow grows with each row. Zuckerman and Lior describe the consequences: asymmetric jet fields, shifted stagnation points, thicker boundary layers and a lower average transfer rate. They identify two mitigations, a smaller jet diameter and more space between jets for the spent flow.[52] Florschuetz et al. arranged their test arrays so that the spent air exited in one direction, which exposes each downstream jet to the crossflow of all the rows before it.[53]

Two later sources describe the effect for architecture choices. Rattner states that conventional arrays extract all spent coolant from the component edges, which produces crossflow interference and nonuniform heat transfer.[54] A patent from International Business Machines states that single-exit drainage scales poorly because the crossflow accumulates.[55] Both statements agree with the correlation evidence in Table 3, and the patent statement is a background assertion without test data.

4.2 Only the Florschuetz correlation includes an explicit crossflow term

Table 3 compares the correlations and datasets that bear on crossflow. The Florschuetz correlation is the only one that expresses the loss as a function of a crossflow ratio. It takes the form Nu/Nu0 = 1 − C (x/d)^nx (y/d)^ny (z/d)^nz (Gc/Gj)^n, where Nu0 is the Nusselt number without crossflow, x/d and y/d are the streamwise and spanwise jet spacings in jet diameters, z/d is the channel height in jet diameters, and Gc/Gj is the ratio of the crossflow mass flux, based on the channel cross-section, to the jet mass flux, based on the hole area.[56] For in-line arrays the constants are C = 0.596, nx = −0.103, ny = −0.380, nz = 0.873 and n = 0.561. For staggered arrays they are C = 1.07, nx = −0.198, ny = −0.406, nz = 0.788 and n = 0.660. The

report fits 2,080 data points with 95 percent within 11 percent.[57]

Table 3. Correlations and datasets that address crossflow in jet arrays

Source	Range of the data	Fluid	Treatment of crossflow	Use for CF-JET
Martin, 1977[58]	Submerged multiple round jets; 2,000 < Re < 100,000; 2 ≤ H/D ≤ 12 (as tabulated in a dissertation)[59]	Gas	Based on arrays with spent-air exits; crossflow not considered	Crossflow-free baseline. The equation was not obtained and is not reproduced.
Florschuetz et al., 1981[60]	In-line x/d 5 to 15, staggered x/d 5 to 10; y/d 4 to 8; z/d 1 to 3; Re about 5×10^3 to 5×10^4; Gc/Gj 0 to 0.8	Air	Multiplier on Nu0 as a function of Gc/Gj and geometry	Quantifies the loss. Liquid use is an extrapolation.
Huber and Viskanta, 1994[6162]	3×3 arrays; Re 3,400 to 20,500; X/D 4 to 8; H/D 0.25 to 6; spent-air exits between jets	Air	Exits remove the crossflow; Nu_f = 0.285 Re^0.710 Pr^0.33 (H/D)^−0.123 (X/D)^−0.725 as reproduced in a dissertation[63]	Small-array exit configuration with a fitted form.
Zuckerman and Lior, 2006[64]	Review; interaction significant at pitch/D < 4 and minor at pitch/D ≥ 8 with H/D ≥ 2	Various	Qualitative description and mitigation	Screening guidance for pitch and diameter.
Rattner, 2017[65]	Simulations; Re 20 to 500; Pr 1 to 100; pitch/D 1.8 to 7.1; more than 1,000 cases	Liquid-like Pr	Interspersed extraction ports; correlations for Nu and pressure-drop k-factors	Laminar range. Coefficients are not in the abstract.
Hobby, 2022[66]	Nine geometries; S/D 2.7 to 9.1; H/D 0.31 to 4.4; Re 70 to 24,000	Pr 0.7 to 21	Interspersed extraction ports; Nu proportional to Re^0.57; 93% of data within ±25%; friction factor mean absolute deviation 20%	Closest published match to the interleaved return-port architecture.

Ranges are those stated in the cited sources. The Florschuetz et al. and Huber and Viskanta datasets are for air. The Prandtl number range of 0.7 to 21 in the Hobby dissertation spans air to water-like fluids, and the 2021 experiments used water.

The other correlations in Table 3 treat crossflow by removing most of it. Their coefficients describe the geometry of the return ports and therefore apply only to that geometry. This distinction affects how CF-JET should use them. The Florschuetz correlation estimates the loss in a one-direction exit array and sets an upper bound on the penalty that interleaved return ports remove. The Hobby correlations describe the architecture that CF-JET proposes and cover Prandtl numbers to 21, which includes water.[67] Figure 3 contrasts a one-direction exit with return ports.

Figure 3. Flow in a conventional jet array and in an array with return ports

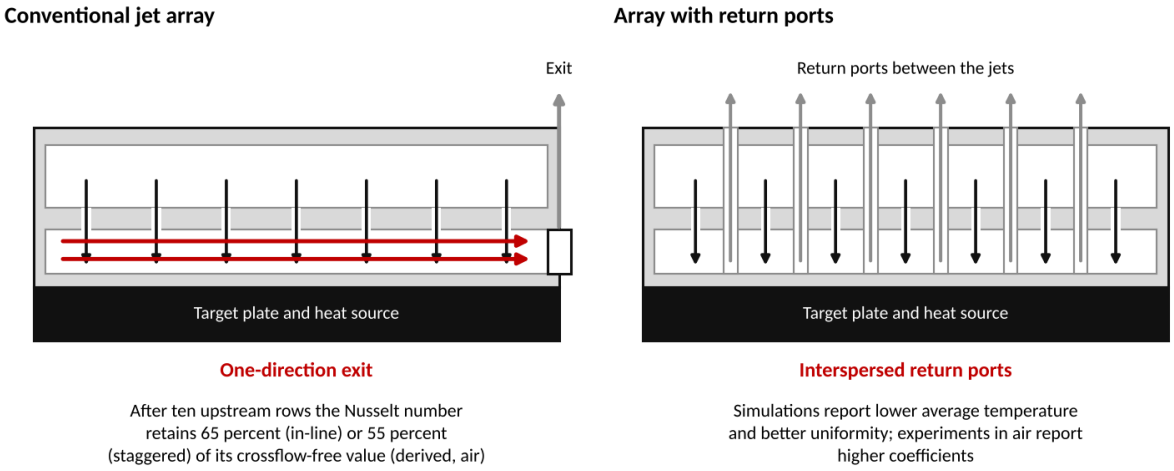

The retention values are derived in this paper from the Florschuetz correlation for air. The effects of return ports are those reported in Table 5. The diagram is schematic and not to scale.

4.3 After ten upstream rows, the correlation predicts a loss of 35 to 45 percent

Table 4 and Figure 4 apply the Florschuetz correlation to arrays that drain to one side. For m upstream rows with equal jet flow, the crossflow ratio at the next row is Gc/Gj = m (π/4)(d/y)(d/z).[68] At x/d = 8, y/d = 6 and z/d = 2, the in-line array retains 0.857 of its crossflow-free Nusselt number after two rows, 0.790 after four rows and 0.648 after ten rows. The staggered array retains 0.845, 0.756 and 0.553 at the same rows.

Table 4. Predicted retention of the crossflow-free Nusselt number in a one-direction exit array (derived)

Array and geometry (x/d, y/d, z/d)	Upstream rows, m	Crossflow ratio Gc/Gj	Nu/Nu0
In-line, 8, 6, 2	2	0.13	0.857
In-line, 8, 6, 2	4	0.26	0.790
In-line, 8, 6, 2	6	0.39	0.736
In-line, 8, 6, 2	10	0.65	0.648
Staggered, 8, 6, 2	2	0.13	0.845
Staggered, 8, 6, 2	4	0.26	0.756
Staggered, 8, 6, 2	6	0.39	0.681
Staggered, 8, 6, 2	10	0.65	0.553
In-line, 8, 6, 1.5	4	0.35	0.808
In-line, 8, 6, 1.5	8	0.70	0.716
In-line, 10, 8, 3	10	0.33	0.703
Staggered, 6, 5, 1.5	6	0.63	0.605

Derived from the Florschuetz et al. simplified correlation with the published constants. All cases lie inside the stated geometry ranges and below Gc/Gj = 0.8. The correlation is fitted to air, and Nu0 is not calculated here.

Figure 4. Predicted retention of the crossflow-free Nusselt number by number of upstream rows

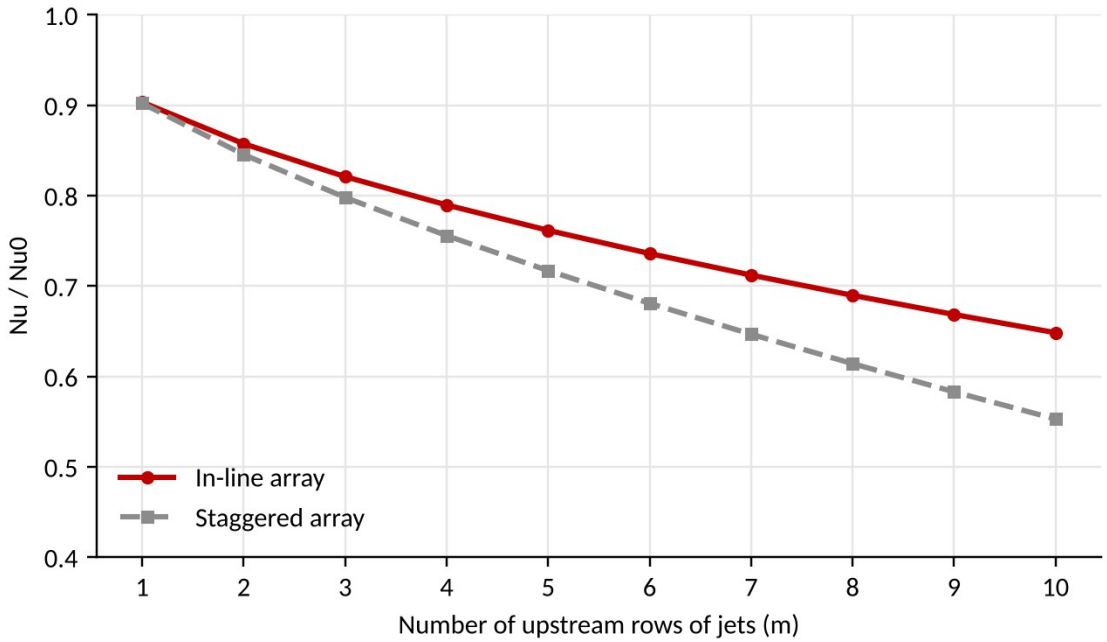

Derived from the Florschuetz et al. correlation at x/d = 8, y/d = 6 and z/d = 2. The correlation is fitted to air. The red line is the in-line array and the grey dashed line is the staggered array.

Three readings follow from Table 4. First, most of the loss accrues in the first rows, because the correlation raises Gc/Gj to the power 0.561 for in-line and 0.660 for staggered arrays: the first upstream row costs about 10 percent and each of rows 8 to 10 about 2 percent (derived). Second, staggered arrays lose more than in-line arrays at the same crossflow ratio once Gc/Gj exceeds about 0.1, which agrees with the report's observation that staggered arrays give lower heat transfer as the spacing decreases and the channel height increases.[69] Third, the channel height has a weak effect on the retained fraction in the range computed: at z/d = 1.5 and eight rows the in-line array retains 0.716, and at z/d = 2 the same eight rows retain 0.690. The lower channel height raises Gc/Gj and lowers the (z/d)^nz term, and the two changes nearly offset.

A crossflow ratio of 0.26 to 0.35 corresponds to retained fractions of 0.76 to 0.81 in Table 4 for the geometries with z/d of 2 and below. A ratio near 0.3 therefore marks the point at which about one fifth of the local coefficient is lost. For the geometry at x/d = 8, y/d = 6 and z/d = 2, a ratio of 0.26 occurs after four rows of jets.

The length of the array sets how far the crossflow develops. At x/d = 8, a 1.0 mm jet gives an 8 mm streamwise pitch and about seven rows across 60 mm, and a 0.5 mm jet gives about fifteen rows (illustrative diameters that are not CF-JET dimensions). Seven upstream rows give Gc/Gj = 0.46 and retained fractions of 0.71 in-line and 0.65 staggered. Twelve upstream rows reach Gc/Gj = 0.79, at the edge of the correlation range, with retained fractions of 0.61 and 0.50 (all derived). At a fixed pitch-to-diameter ratio, a smaller jet diameter raises the number of rows in a fixed footprint and the loss in the last row. The mitigation that Zuckerman and Lior give, a smaller diameter with more space between jets, applies at a fixed pitch, which raises x/d and y/d.[70]

4.4 The correlation limits what the estimate shows about CF-JET

The Florschuetz correlation was fitted to air at Reynolds numbers of about 5×10^3 to 5×10^4 and depends on

the Prandtl number only through a Pr^(1/3) factor.[71] The CF-JET coolant is 50/50 water-glycol at 65 °C, and the jet Reynolds number depends on the nozzle diameter and count, which the sources reviewed do not give. The estimates in Table 4 therefore indicate the direction and approximate size of the loss in an air array. Huber and Viskanta tested a 3×3 array with spent-air exits, and Rattner simulated laminar flows from Re = 20 to 500. Neither dataset covers a water-glycol array at the design flow of 4 to 8 L/min.[7273]

5. Return-Port and Manifold Architectures

5.1 Interspersed extraction ports reduce crossflow in air and liquid studies

Table 5 summarizes the architectures that the sources reviewed tested against single-exit arrays. Huber and Viskanta found that spent-air exits between the jets of a confined 3×3 array raised the heat transfer coefficient and moved the optimum nozzle spacing, and Huber concluded in a dissertation that removing crossflow is the main benefit of exits for all but small separation distances.[7475] Rattner simulated more than 1,000 cases with interspersed extraction ports and reported lower average temperatures, better uniformity and modest pressure drops, with correlations for Nusselt number and pressure-drop loss coefficients.[76] The abstract does not give the numerical values of the gain.

The footprints stated in the sources of Tables 2 and 5 range from 1 to 6.5 cm², with Brunschwiler et al. describing a distributed return scaled to 40,000 cells on 4 cm².[77] The CF-JET footprint of 36 cm² is 5.6 times the largest stated footprint (derived), and no source reviewed demonstrates an interleaved return array of that size with water-glycol.

Table 5. Return-port and manifold architectures and the effects reported

Architecture	Source	Reported effect	Basis and caveat
Single-edge exit	Rattner; U.S. Patent 8,413,712[7879]	Crossflow interference and nonuniform heat transfer; scales poorly as crossflow accumulates	Review statement and patent background
Spent-air exits between jets, 3×3 array	Huber and Viskanta, 1994[80]	Exits raised the coefficient and moved the optimum separation	Air; experiment
Interspersed extraction ports	Rattner, 2017[81]	Lower average temperature, better uniformity, modest pressure drop	Simulation; laminar Re 20 to 500
Interspersed ports, water, 3D-printed	Hobby et al., 2021[82]	Pressure drop matched after manifold losses were added; heat transfer matched reasonably with differing trends	Photopolymer device; experiment and simulation
Interspersed ports, nine geometries	Hobby, 2022[83]	Correlations for Nu and friction factor; low S/D is efficient and less effective, high S/D is effective and less efficient	Experiment
Micron-scale distributed return	Brunschwiler et al., 2006[84]	Jets of 31 to 126 µm at 100 to 500 µm pitch; parallel inlet and outlet manifolds scale to 40,000 cells on 4 cm²	Silicon-scale; experiment
Effusion holes in the jet plate	Zuckerman and Lior, citing Rhee et al.[85]	50% improvement in array-average transfer at H/D = 0.5	Review of air results
Manifold microchannel	Collins et al., 2019[86]	Pressure drop reduced by about 90% at Re near 210 and 40% near 1,175; resistance higher than straight channels	Additively manufactured; experiment

Architecture	Source	Reported effect	Basis and caveat
Multi-inlet and multi-outlet manifold on pin fins	Journal of Electronic Packaging, 2022[87]	Three-channel manifold cut resistance from 0.061 to 0.054 °C/W and lowered pressure drop by 0.77 kPa; seven-channel design cut resistance by 16.4% with pressure drop below 0.6 kPa	Largely numerical

The Hobby et al. photopolymer device and the Collins et al. manifold are the two tests of 3D-printed return geometry that the sources reviewed describe. Resistance values are as reported by each source.

5.2 Manifold losses account for a large share of the pressure drop

Hobby et al. found that the measured pressure drop of their 3D-printed water device agreed with simulation only after the manifold losses were modeled, and their heat transfer comparison agreed reasonably with differing trends.[88] Wei reports that the outlet plenum accounted for 57 percent of the total pressure drop at 1,000 mL/min in a polymer multi-jet cooler, a result from a different scale and material than CF-JET.[89] The CF-JET design point sets the pressure drop at 30 kPa or less, and the manifold and return passages share that allowance with the jets. The sources reviewed give no pressure drop budget for an interleaved printed plate at the 4 to 8 L/min flows of the design point.

5.3 Return ports trade stagnation area for crossflow relief

Each return port removes area that a jet could cool and shortens the path of the spent fluid. Hobby's correlations show the trade in terms of spacing: small S/D gives efficient and less effective cooling and large S/D gives effective and less efficient cooling.[90] The CF-JET design chooses a point on that curve for each die. The sources reviewed give no data on the spreading that a target plate must supply between stagnation regions when return ports occupy part of the surface.

6. Mass Scaling of Cold Plates

6.1 Copper has 3.3 times the density of aluminum and a lower conductivity per unit mass than an aluminum alloy

Table 6 compares the materials that appear in the cold plate literature. A 60 mm by 60 mm by 3 mm plate has a volume of 10.8 cm^3 and a mass of 96 g in copper and 29 g in AlSi10Mg.[91] The thermal conductivity per unit density is 44.5 for copper, 42.8 for the copper alloy and 51.9 for AlSi10Mg in W/m·K per g/cm^3, so the printed aluminum alloy conducts 17 percent more per unit mass than copper even though its absolute conductivity is lower by a factor of 2.8.[9293]

Table 6. Density, conductivity and mass of cold plate materials (derived values as marked)

Material	Density (g/cm^3)	Conductivity (W/m·K)	Conductivity per density (derived)	Mass of 60×60×3 mm plate, g (derived)	Conduction resistance, 3 mm, mm^2·K/W (derived)
Copper[94]	8.92 (8.89 standard)	397	44.5	96	7.6
Copper alloy, printed[95]	8.89	380.2	42.8	96	7.9
AlSi10Mg, printed	2.7	140	51.9	29	21.4

Copper values are from the Copper Development Association. Printed alloy values are from the material table of Hoang et al., which is a

numerical comparison. Collins et al. report 110 W/m·K for printed AlSi10Mg. The conduction resistance is the thickness divided by the conductivity. Conductivity of wrought aluminum alloys was not obtained from a citable source in this review.

The through-thickness conduction of a 3 mm plate consumes 7.6 mm²·K/W in copper and 21.4 mm²·K/W in AlSi10Mg (derived). Against the 72 mm²·K/W target, that is 11 percent and 30 percent of the resistance budget before any spreading, jet convection or interface resistance is counted. A lighter plate costs conduction resistance in proportion, and the cost is largest for the aluminum alloy. Figure 5 shows the share of the budget.

Figure 5. Conduction resistance of a 3 mm plate against the 72 mm²·K/W target (derived)

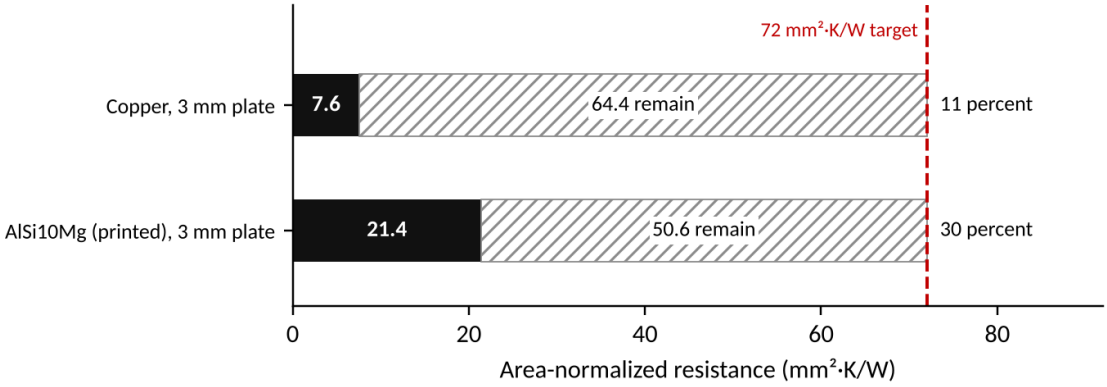

Conduction resistance is the thickness divided by the conductivity in Table 6.

6.2 Construction outside the conduction path accounts for much of the assembled mass

An NREL light-weight cold plate study reports that a glass-fiber reinforced nylon design saves about 2.9 kg, roughly 50 percent of the mass, which implies a baseline near 5.8 kg (derived).[96] The page gives no absolute mass. Modeled gains in the same study reached 79 percent in power density and 118 percent in specific power. A Raytheon patent states in its background that aluminum cold plates are a major contributor to the weight of active electronically scanned array systems and proposes reinforced plastic plates to cut it.[97] Both sources indicate that mass is a system-level quantity in which construction, housing and coolant inventory matter alongside the plate material.

No public dataset found in this review links cold plate mass to thermal resistance for ground vehicle or aerospace applications. The relationships that can be stated are the density and conductivity arithmetic in Table 6 and the NREL and patent statements above. A mass-performance comparison for CF-JET requires the mass of the finished assembly, the conductance in W/K and the pressure drop at a stated flow.

The target of 0.02 K/W equals a conductance of 50 W/K. A report of conductance per unit mass allows assemblies of different size to be compared: 50 W/K at 1 kg gives 50 W/K per kg, and the same conductance at 2 kg gives 25 W/K per kg (illustrative). The metric combines the two quantities that the Raytheon patent and the NREL study treat separately, resistance and mass.[9899] Reporting the pair for each candidate in the CF-JET trade space gives the program office a single comparison basis across the cold plate options.

7. Evaluation of the Three Claims

7.1 The density values are supported

The Copper Development Association gives the standard density of copper as 8.89 g/cm³ and the typical value at 20 °C as 8.92 g/cm³, a difference of 0.3 percent.[100] Hoang et al. list 8.89 g/cm³ for a copper alloy and 2.7 g/cm³ for AlSi10Mg.[101] The ratio of copper to the printed aluminum alloy is 3.3. A wrought aluminum density from a citable source was not obtained in this review, and the sourced aluminum value applies to the printed alloy.

7.2 The jet claim holds for local coefficients and needs two qualifications

Local jet coefficients of 210 to 250 kW/m²·K and the factor of up to three over channel flow support the claim at the point of impingement.[102][103][104] Two qualifications apply. The area-averaged coefficient in the Oak Ridge study is 6.34 kW/m²·K, which is a ratio of about 33 below the local value.[105] Single-phase microchannels and microtubes have also reached 790 W/cm² for silicon microchannels and about 3,000 W/cm² for water in microtubes, and a hybrid microchannel and slot-jet module reached 305.9 W/cm² without phase change.[106][107] The claim holds for local coefficient and does not extend to peak heat flux, where microchannel and microtube results are at least as high.

7.3 The 0.02 K/W target is aggressive against conventional plates and inside published jet results

The target of 0.02 K/W at 1.5 kW is a 30 K rise from case to coolant. On the 36 cm² footprint it equals 0.72 K·cm²/W, or 72 mm²·K/W, and an effective coefficient of about 13.9 kW/m²·K.[108] The average heat flux is 41.7 W/cm². Table 7 compares the target with the references in Table 2. It is better than the swaged-tube and finned figures by factors of 2.8 and 1.4. It lies within the range of the Collins et al. microchannels (42 to 94 mm²·K/W) and allows 1.7 to 8 times the resistance of the other additively manufactured, jet and microchannel results.

Table 7. CF-JET resistance target as a multiple of published area-normalized resistance (derived)

Reference	Resistance (mm²·K/W)	Target as a multiple of the reference
Swaged-tube cold plate, patent background	200	0.36
Finned cold plate, patent background	100	0.72
Manifold microchannel, AlSi10Mg (Collins et al.)	65 to 94	0.77 to 1.1
Straight microchannel, AlSi10Mg (Collins et al.)	42 to 72	1.0 to 1.7
Impingement pin fin, aluminum alloy (Hoang et al.)	41 to 43	1.7
Impingement pin fin, copper alloy (Hoang et al., numerical)	31	2.3
Hotspot micro pin fins (Fallahtafti et al., numerical)	21	3.5
Jet array on AlSiC plate (Pahinkar et al., numerical)	17.5	4.1
Jet impingement, convective path (NREL)	Below 20	Above 3.6
SiC half-bridge module with jets, junction-to-fluid (NREL)	About 15	4.8
Silicon microchannel (Tuckerman and Pease)	9	8.0

A multiple above 1 means that the target allows more resistance than the reference achieved. Values from Table 2. The reference values use different areas, fluids and reference planes.

Table 8 gives the operating quantities at the design point. At 4 to 8 L/min the coolant bulk rise is 6.1 to 3.1

K, which uses 10 to 20 percent of the 30 K budget if the case-to-coolant resistance is referenced to the inlet temperature.[109] The hydraulic power at 30 kPa is 2 to 4 W.

Flow per unit footprint area gives a second check. The Hoang et al. aluminum plate used 2 L/min on 6.45 cm^2, which is 0.31 L/min per cm^2, and their copper alloy case used 1 L/min, or 0.16 L/min per cm^2.[110] The CF-JET design flow of 4 to 8 L/min on 36 cm^2 is 0.11 to 0.22 L/min per cm^2 (derived). That is 0.36 to 0.72 times the flow per area of the aluminum plate and 0.72 to 1.4 times that of the copper alloy case, while the 30 kPa allowance exceeds the 8.14 kPa of the copper alloy case and the 21.1 to 28.1 kPa of the aluminum plate. Published plates with comparable flow per area reached 31 to 43 mm^2·K/W, which is a factor of 1.7 to 2.3 below the target resistance.

The comparison has a limit. The Hoang et al. plates were modeled with a different coolant and a smaller footprint, and their resistances are numerical results.[111] The CF-JET design operates with 50/50 water-glycol at 65 °C, whose viscosity is higher and whose thermal conductivity is lower than those of water at room temperature, and both properties lower the jet coefficient at equal velocity.[112] The comparison therefore indicates the order of magnitude of the flow needed, and the CF-JET flow range of 4 to 8 L/min is within that order.

Table 8. Operating quantities at the CF-JET design point (derived)

Quantity	4 L/min	6 L/min	8 L/min
Coolant mass flow (kg/s)	0.069	0.104	0.138
Coolant bulk rise at 1.5 kW (K)	6.1	4.1	3.1
Share of the 30 K budget (%)	20	14	10
Hydraulic power at 30 kPa (W)	2	3	4

Derived from a density of 1,038 kg/m^3 and a specific heat of 3.53 kJ/kg·K for 50% glycol in DOWTHERM SR-1 at 180 °F (82 °C). The specification does not list values at the 65 °C inlet, so the values are an approximation. Hydraulic power is flow times pressure drop.

The claim holds with a condition. The target is credible for the convective path because published jet results of 15 to 20 mm^2·K/W leave a margin of 3.6 to 4.8 times. The target is demanding when the case reference plane lies on the module side of the stack, because the spreading, interface and plate conduction resistances add to the convective term, and a 3 mm aluminum alloy plate alone uses 30 percent of the budget (Table 6). If the heat enters through dies that cover a fraction of the footprint, the heat flux at the die is higher than the 41.7 W/cm^2 average by the inverse of that fraction. The definition of the case reference plane in the CF-JET proposal was not available for this review, and the verdict depends on it.

8. Implications for the CF-JET Effort

The published record supports the CF-JET premise that jets on an interleaved-return plate can reach resistances well below conventional cold plates, and it leaves the combination that CF-JET proposes untested: a printed manifold with interleaved ports, a carbon fiber target plate with perpendicular inserts and a plated coolant face at a flow of 4 to 8 L/min of water-glycol.[113] The independent evidence in Tables 2 and 5 covers jets, return ports and printed plates separately.

The record supports three statements that the program can use. Jets reach convective resistances of 15 to 20 mm^2·K/W in published results, which is 3.6 to 4.8 times below the target resistance (Table 7). Crossflow accounts for a loss of up to about 45 percent in the local coefficient of a long one-direction array, and return ports are the documented remedy (Tables 4 and 5). Mass depends on construction as well as on

plate metal (Table 6). The record does not establish the thermal resistance of a printed, interleaved-return plate with a carbon fiber target at 36 cm² and a flow of 4 to 8 L/min.

8.1 Six risks follow from the evidence

- **Case reference plane.** The 0.02 K/W target equals 72 mm²·K/W, and the published values in Table 7 refer to different parts of the thermal path. A target stated without its reference plane cannot be verified against any of them.
- **Crossflow in the array.** At the geometry computed, an array that drains to one side loses 35 to 45 percent of the local Nusselt number after ten upstream rows (derived from an air correlation). Interspersed returns remove most of that loss in the studies reviewed, and no study covers water-glycol at the design flow.
- **Local and average coefficients.** The Oak Ridge result of 210 kW/m²·K local and 6.34 kW/m²·K averaged shows that the stagnation value overstates the convective term by a ratio near 33. The spreading that the carbon fiber target plate provides between jets governs the average.
- **Printed material properties.** Printed AlSi10Mg shows 110 to 140 W/m·K and a surface roughness near 20 µm in the studies reviewed, and the body conductivity and the surface of the return passages affect both conduction and pressure drop.[114][115]
- **Pressure drop budget.** Manifold losses had to be modeled to match the pressure drop of the printed water device, and an outlet plenum took 57 percent of the drop in a polymer cooler.[116][117] The 30 kPa limit covers the manifold, return passages and jets together.
- **Plated face and jet erosion.** NREL's 180-day reliability test observed unchanged nozzle diameters and oxidation.[118] No source reviewed tests a thin plated face on a carbon fiber plate under jets, so the durability of that face at the design velocity has no published evidence.

8.2 Seven design implications for the program

- **Define the reference plane.** State where the case temperature is measured and report resistance in K/W and in mm²·K/W with the area, so that results can be set against Table 7.
- **Limit the crossflow ratio.** Place return ports so that Gc/Gj stays at or below about 0.3, which corresponds to a port at least every three to four rows at the geometries in Table 4.
- **Use the interspersed-port correlations.** Apply the Hobby correlations for Nusselt number and friction factor to the CF-JET geometry, with the Florschuetz form as the estimate for the loss in any section that drains to one side.[119][120]
- **Specify material by conductance and mass.** Report the conductance in W/K, the mass of the finished assembly and the specific conductance in W/K per kg, because the density arithmetic in Table 6 and the NREL manifold result show that plate metal alone does not set mass.
- **Budget the pressure drop by component.** Allocate the 30 kPa among the manifold, return passages and jets, and measure the plenum pressure at the design flows.
- **Test a representative sub-array.** Map the local coefficient of a multi-row array with water-glycol at 65 °C and 4 to 8 L/min, with and without return ports, so that the crossflow loss is measured for the coolant in use.
- **Measure the finished plate.** Measure the conductivity of the printed body and the through-thickness conduction of the carbon fiber target plate, since a 3 mm aluminum alloy plate would use 30 percent of the budget.

8.3 Six research questions remain open

- Where does the CF-JET proposal place the case reference plane, and what stack and spreading resistance does it include?
- How much of the 35 to 45 percent air-based crossflow loss appears in water-glycol at the Prandtl and Reynolds numbers of the design point?
- What area-averaged coefficient does the CF-JET plate achieve against its local value, and what in-plane spreading does the carbon fiber target plate supply between jets?
- What fraction of the 30 kPa budget do the manifold and return passages consume at 4, 6 and 8 L/min?
- How do the mass and conductance of the CF-JET assembly compare with copper and AlSi10Mg plates with the same manifold?
- Does a thin plated coolant face on the target plate withstand jet erosion over the design life?

9. Conclusion

Conventional machined and brazed cold plates reach 100 to 200 mm^2·K/W in the finned and swaged-tube forms, and printed microchannel, pin-fin and jet plates reach 31 to 94 mm^2·K/W in peer-reviewed work. The CF-JET target of 0.02 K/W at 1.5 kW equals 72 mm^2·K/W, which is aggressive against conventional plates and inside the published jet and microchannel results, with the case reference plane deciding whether it holds.

Jets have the highest local coefficients of the single-phase methods reviewed and a far lower area-averaged coefficient. Crossflow reduces downstream transfer, and the Florschuetz correlation predicts a loss of 35 to 45 percent after ten upstream rows in air. Interspersed return ports reduce the loss in the studies reviewed, and manifold losses account for a large share of the pressure drop in the printed water device tested. Copper has 3.3 times the density of aluminum, and construction outside the conduction path accounts for much of the assembled mass in the NREL study.

The CF-JET effort can add the evidence that is missing: a defined reference plane, a measured crossflow loss with water-glycol at the design flow, a pressure drop budget by component and a mass and conductance report for the finished plate.

Bibliography

Barua, Himel, Emre Gurpinar, Lingxiao Xue, and Burak Ozpineci. “Comparative Analysis of Direct and Indirect Cooling of Wide-Bandgap Power Modules and Performance Enhancement of Jet Impingement-Based Direct Substrate Cooling.” Draft paper IPACK2022-97172. ASME InterPACK2022, Anaheim, CA, 24–28 October 2022. https://www.osti.gov/biblio/1908080.

Brunschwiler, Thomas, et al. “Direct Liquid Jet-Impingement Cooling with Micron-Sized Nozzle Array and Distributed Return Architecture.” In *2006 10th IEEE Intersociety Conference on Thermal and Thermomechanical Phenomena in Electronics Systems (ITherm)*, 196–203. 2006.

Collins, Ivel L., Justin A. Weibel, Liang Pan, and Suresh V. Garimella. “Evaluation of Additively Manufactured Microchannel Heat Sinks.” *IEEE Transactions on Components, Packaging and Manufacturing Technology* (2019). https://doi.org/10.1109/TCPMT.2018.2866972.

Copper Development Association. “Introduction to Copper: Fact Sheets.” Copper.org. https://copper.org/publications/newsletters/innovations/2001/08/intro_fac.php.

The Dow Chemical Company. *DOWTHERM SR-1 Heat Transfer Fluid: Engineering Specifications for Closed-Loop HVAC Systems*. Vendor specification, n.d. https://www.deppmann.com/wp-content/uploads/2016/08/DowTherm-SR-1-Specification.pdf.

Fallahtafti, Najmeh, et al. “Shape Optimization of Hotspot Targeted Micro Pin Fins for Heterogeneous Integration Applications.” *International Journal of Heat and Mass Transfer* 192 (2022): 122897.

Florschuetz, L. W., D. E. Metzger, and C. R. Truman. “Jet Array Impingement with Crossflow: Correlation of Streamwise Resolved Flow and Heat Transfer Distributions.” NASA Contractor Report CR-3373 (ERC-R-80024). Arizona State University, January 1981. https://ntrs.nasa.gov/citations/19810006721.

Hoang, Cong Hiep, et al. “Design and Thermal Analysis of a 3-D Printed Impingement Pin Fin Cold Plate for Heterogeneous Integration Application.” *IEEE Transactions on Components, Packaging and Manufacturing Technology* (2022). https://doi.org/10.1109/TCPMT.2022.3185401.

Hobby, David, Tom Walker, Alex Rattner, Chris Jacobsen, David Sherrer, and Todd Bandhauer. “Comparison of Experimental and Computational Heat Transfer Characterization of Water Jet Impingement Array with Interspersed Fluid Extraction.” *Heat Transfer Engineering* (2021). https://doi.org/10.1080/01457632.2019.1707404.

Hobby, David Ryan. “Generalized Pressure Drop and Heat Transfer Correlations for Jet Impingement Cooling with Jet Adjacent Fluid Extraction.” PhD diss., Colorado State University, 2022. https://mountainscholar.org/handle/10217/235294.

Huber, Aaron M., and Raymond Viskanta. “Effect of Jet-Jet Spacing on Convective Heat Transfer to Confined, Impinging Arrays of Axisymmetric Air Jets.” *International Journal of Heat and Mass Transfer* 37, no. 18 (1994): 2859–2869. https://doi.org/10.1016/0017-9310(94)90340-9.

Huber, Aaron M., and Raymond Viskanta. “Convective Heat Transfer to a Confined Impinging Array of Air Jets with Spent Air Exits.” *Journal of Heat Transfer* 116, no. 3 (1994): 570–576.

Huber, Aaron Morgan. “Heat Transfer with Impinging Gaseous Jet Systems.” PhD diss., Purdue University, n.d. https://docs.lib.purdue.edu/dissertations/AAI9420845.

Martin, Holger. “Heat and Mass Transfer between Impinging Gas Jets and Solid Surfaces.” *Advances in Heat Transfer* 13 (1977): 1–60.

Moreno, Gilbert. *Power Electronics Thermal Management R&D: Annual Report*. NREL/MP-5400-64943. National Renewable Energy Laboratory, April 2016. https://www.nrel.gov/docs/fy16osti/64943.pdf.

Narumanchi, Sreekant. “Light-Weight, Single-Phase, Liquid-Cooled Cold Plate.” National Renewable Energy Laboratory, U.S. Department of Energy Office of Energy Efficiency and Renewable Energy, 15 May 2012. https://www.energy.gov/eere/vehicles/articles/compact-light-weight-single-phase-liquid-cooled-cold-plate-0.

Pahinkar, Darshan G., Lauren Boteler, Dimeji Ibitayo, Sreekant Narumanchi, Paul Paret, Douglas DeVoto, Joshua Major, and Samuel Graham. “Liquid Cooled Aluminum Silicon Carbide Heat Sinks for Reliable Power Electronics Packages.” Accepted manuscript, U.S. Department of Energy Public Access, undated. https://www.osti.gov/servlets/purl/1507288.

Rattner, Alexander S. “General Characterization of Jet Impingement Array Heat Sinks with Interspersed Fluid Extraction Ports for Uniform High-Flux Cooling.” *Journal of Heat Transfer* 139, no. 8 (August 2017): 082201. https://doi.org/10.1115/1.4036090.

SOL Engineering Services, LLC. *CF-JET: AI/ML-Enabled Design and Development of an Additively Manufactured, Liquid-Cooled Jet-Impingement Cold Plate with Optimized Carbon Fiber Target Plate*. Proposal, Rev Final 2, n.d.

Sung, Myung Ki, and Issam Mudawar. “Single-Phase and Two-Phase Cooling Using Hybrid Micro-Channel/Slot-Jet

Module.” *International Journal of Heat and Mass Transfer* 51 (2008): 3825–3839. https://engineering.purdue.edu/mudawar/files/articles-all/2008/2008-02.pdf.

“Thermal Optimization and Experimental Demonstration of a Silicon Carbide, Half-Bridge Power Module.” *Advancing Microelectronics* 52, no. 4 (2025): 22–27. NREL Research Hub record. https://research-hub.nrel.gov/en/publications/thermal-optimization-and-experimental-demonstration-of-a-silicon-/.

Tuckerman, D. B., and R. F. W. Pease. “High-Performance Heat Sinking for VLSI.” *IEEE Electron Device Letters* EDL-2, no. 5 (May 1981): 126–129.

“Thermal Management System and Method for Electronic Equipment Mounted on Coldplates.” U.S. Patent 7,092,255. Raytheon Company, granted 15 August 2006. https://patents.google.com/patent/US7092255B2/en.

“Cooling Device.” U.S. Patent 8,413,712. International Business Machines Corporation, granted 9 April 2013. https://patents.google.com/patent/US8413712B2/en.

“Heat Exchanger Having Winding Micro-Channels.” U.S. Patent 8,474,516. Mikros Manufacturing Inc., granted 2 July 2013. https://patents.google.com/patent/US8474516B2/en.

“Using a Multi-Inlet/Outlet Manifold to Improve Heat Transfer and Flow Distribution of a Pin Fin Heat Sink.” *Journal of Electronic Packaging* 144, no. 3 (September 2022): 031017. https://doi.org/10.1115/1.4054461.

Walsh, Stephen Michael. “Microjet Impingement Cooling of High Power-Density Electronics.” SM thesis, Massachusetts Institute of Technology, 2018. http://hdl.handle.net/1721.1/118677.

Waye, Scot K., Sreekant Narumanchi, Mark Mihalic, Gilbert Moreno, Kevin Bennion, and Jana Jeffers. “Advanced Liquid Cooling for a Traction Drive Inverter Using Jet Impingement and Microfinned Enhanced Surfaces.” Preprint NREL/CP-5400-61060. Presented at ITherm 2014, Orlando, FL, 27–30 May 2014. National Renewable Energy Laboratory, August 2014. https://www.osti.gov/biblio/1150183.

Waye, Scot, Sreekant Narumanchi, and Gilbert Moreno. “Traction Drive Inverter Cooling with Submerged Liquid Jet Impingement on Microfinned Enhanced Surfaces.” Presentation, National Renewable Energy Laboratory, 2014. https://research-hub.nrel.gov/en/publications/traction-drive-inverter-cooling-with-submerged-liquid-jet-impinge/.

Wei, Tiwei. “High Efficiency Polymer based Direct Multi-jet Impingement Cooling Solution for High Power Devices.” arXiv:2310.11663. Preprint submitted 18 October 2023. https://arxiv.org/abs/2310.11663.

Zuckerman, Neil, and Noam Lior. “Jet Impingement Heat Transfer: Physics, Correlations, and Numerical Modeling.” *Advances in Heat Transfer* 39 (2006): 565–631. https://doi.org/10.1016/S0065-2717(06)39006-5.

Notes

[1]SOL Engineering Services, LLC, *CF-JET: AI/ML-Enabled Design and Development of an Additively Manufactured, Liquid-Cooled Jet-Impingement Cold Plate with Optimized Carbon Fiber Target Plate*, proposal, Rev Final 2, n.d.

[2]"Heat Exchanger Having Winding Micro-Channels," U.S. Patent 8,474,516, Mikros Manufacturing Inc., granted 2 July 2013, https://patents.google.com/patent/US8474516B2/en.

[3]Gilbert Moreno, *Power Electronics Thermal Management R&D: Annual Report*, NREL/MP-5400-64943, National Renewable Energy Laboratory, April 2016, https://www.nrel.gov/docs/fy16osti/64943.pdf.

[4]U.S. Patent 8,474,516.

[5]Ivel L. Collins, Justin A. Weibel, Liang Pan, and Suresh V. Garimella, "Evaluation of Additively Manufactured Microchannel Heat Sinks," *IEEE Transactions on Components, Packaging and Manufacturing Technology* (2019), https://doi.org/10.1109/TCPMT.2018.2866972.

[6]Cong Hiep Hoang et al., "Design and Thermal Analysis of a 3-D Printed Impingement Pin Fin Cold Plate for Heterogeneous Integration Application," *IEEE Transactions on Components, Packaging and Manufacturing Technology* (2022), https://doi.org/10.1109/TCPMT.2022.3185401.

[7]Neil Zuckerman and Noam Lior, "Jet Impingement Heat Transfer: Physics, Correlations, and Numerical Modeling," *Advances in Heat Transfer* 39 (2006): 565–631, p. 566, https://doi.org/10.1016/S0065-2717(06)39006-5.

[8]Himel Barua, Emre Gurpinar, Lingxiao Xue, and Burak Ozpineci, "Comparative Analysis of Direct and Indirect Cooling of Wide-Bandgap Power Modules and Performance Enhancement of Jet Impingement-Based Direct Substrate Cooling," draft paper IPACK2022-97172, ASME InterPACK2022, Anaheim, CA, 24–28 October 2022, https://www.osti.gov/biblio/1908080.

[9]D. B. Tuckerman and R. F. W. Pease, "High-Performance Heat Sinking for VLSI," *IEEE Electron Device Letters* EDL-2, no. 5 (May 1981): 126–129.

[10]Myung Ki Sung and Issam Mudawar, "Single-Phase and Two-Phase Cooling Using Hybrid Micro-Channel/Slot-Jet Module," *International Journal of Heat and Mass Transfer* 51 (2008): 3825–3839, https://engineering.purdue.edu/mudawar/files/articles-all/2008/2008-02.pdf.

[11]L. W. Florschuetz, D. E. Metzger, and C. R. Truman, "Jet Array Impingement with Crossflow: Correlation of Streamwise Resolved Flow and Heat Transfer Distributions," NASA Contractor Report CR-3373 (ERC-R-80024), Arizona State University, January 1981, https://ntrs.nasa.gov/citations/19810006721.

[12]Alexander S. Rattner, "General Characterization of Jet Impingement Array Heat Sinks with Interspersed Fluid Extraction Ports for Uniform High-Flux Cooling," *Journal of Heat Transfer* 139, no. 8 (August 2017): 082201, https://doi.org/10.1115/1.4036090.

[13]Aaron M. Huber and Raymond Viskanta, "Convective Heat Transfer to a Confined Impinging Array of Air Jets with Spent Air Exits," *Journal of Heat Transfer* 116, no. 3 (1994): 570–576.

[14]David Hobby, Tom Walker, Alex Rattner, Chris Jacobsen, David Sherrer, and Todd Bandhauer, "Comparison of Experimental and Computational Heat Transfer Characterization of Water Jet Impingement Array with Interspersed Fluid Extraction," *Heat Transfer Engineering* (2021), https://doi.org/10.1080/01457632.2019.1707404.

[15]Sreekant Narumanchi, "Light-Weight, Single-Phase, Liquid-Cooled Cold Plate," National Renewable Energy Laboratory, U.S. Department of Energy Office of Energy Efficiency and Renewable Energy, 15 May 2012, https://www.energy.gov/eere/vehicles/articles/compact-light-weight-single-phase-liquid-cooled-cold-plate-0.

[16]Copper Development Association, "Introduction to Copper: Fact Sheets," Copper.org, https://copper.org/publications/newsletters/innovations/2001/08/intro_fac.php.

[17]Hoang et al., "3-D Printed Impingement Pin Fin Cold Plate."

[18]Barua et al., "Comparative Analysis of Direct and Indirect Cooling."

[19]Stephen Michael Walsh, "Microjet Impingement Cooling of High Power-Density Electronics," SM thesis, Massachusetts Institute of Technology, 2018, http://hdl.handle.net/1721.1/118677.

[20]Tuckerman and Pease, "High-Performance Heat Sinking for VLSI."

[21]Sung and Mudawar, "Hybrid Micro-Channel/Slot-Jet Module."

[22]U.S. Patent 8,474,516.

[23]Moreno, *Power Electronics Thermal Management R&D*.

[24]SOL Engineering Services, *CF-JET*, Rev Final 2.

[25]SOL Engineering Services, *CF-JET*, Rev Final 2.

[26]U.S. Patent 8,474,516.

[27]Tuckerman and Pease, "High-Performance Heat Sinking for VLSI."

[28]U.S. Patent 8,474,516.

[29]Hoang et al., "3-D Printed Impingement Pin Fin Cold Plate."

[30]Najmeh Fallahtafti et al., "Shape Optimization of Hotspot Targeted Micro Pin Fins for Heterogeneous Integration Applications," *International*

Journal of Heat and Mass Transfer 192 (2022): 122897.

[31]Darshan G. Pahinkar, Lauren Boteler, Dimeji Ibitayo, Sreekant Narumanchi, Paul Paret, Douglas DeVoto, Joshua Major, and Samuel Graham, "Liquid Cooled Aluminum Silicon Carbide Heat Sinks for Reliable Power Electronics Packages," accepted manuscript, U.S. Department of Energy Public Access, undated, https://www.osti.gov/servlets/purl/1507288.

[32]Moreno, *Power Electronics Thermal Management R&D*.

[33]"Thermal Optimization and Experimental Demonstration of a Silicon Carbide, Half-Bridge Power Module," *Advancing Microelectronics* 52, no. 4 (2025): 22–27, NREL Research Hub record, https://research-hub.nrel.gov/en/publications/thermal-optimization-and-experimental-demonstration-of-a-silicon-/.

[34]Barua et al., "Comparative Analysis of Direct and Indirect Cooling."

[35]SOL Engineering Services, *CF-JET*, Rev Final 2.

[36]Collins et al., "Additively Manufactured Microchannel Heat Sinks."

[37]Hoang et al., "3-D Printed Impingement Pin Fin Cold Plate."

[38]Collins et al., "Additively Manufactured Microchannel Heat Sinks."

[39]Derived in this paper as the reciprocal of the convective share of 72 $mm^2 \cdot K/W$: $1 \div 72 \times 10^{-6} = 13{,}889\ W/m^2 \cdot K$; $1 \div 54 \times 10^{-6} = 18{,}519\ W/m^2 \cdot K$; $1 \div 36 \times 10^{-6} = 27{,}778\ W/m^2 \cdot K$.

[40]Pahinkar et al., "Liquid Cooled Aluminum Silicon Carbide Heat Sinks."

[41]Barua et al., "Comparative Analysis of Direct and Indirect Cooling."

[42]SOL Engineering Services, *CF-JET*, Rev Final 2.

[43]Zuckerman and Lior, "Jet Impingement Heat Transfer," p. 566.

[44]Zuckerman and Lior, "Jet Impingement Heat Transfer," p. 573.

[45]Walsh, "Microjet Impingement Cooling."

[46]Barua et al., "Comparative Analysis of Direct and Indirect Cooling."

[47]Barua et al., "Comparative Analysis of Direct and Indirect Cooling."

[48]Zuckerman and Lior, "Jet Impingement Heat Transfer," pp. 579–581.

[49]Scot K. Waye, Sreekant Narumanchi, Mark Mihalic, Gilbert Moreno, Kevin Bennion, and Jana Jeffers, "Advanced Liquid Cooling for a Traction Drive Inverter Using Jet Impingement and Microfinned Enhanced Surfaces," preprint NREL/CP-5400-61060, presented at ITherm 2014, Orlando, FL, 27–30 May 2014, National Renewable Energy Laboratory, August 2014, https://www.osti.gov/biblio/1150183.

[50]Scot Waye, Sreekant Narumanchi, and Gilbert Moreno, "Traction Drive Inverter Cooling with Submerged Liquid Jet Impingement on Microfinned Enhanced Surfaces," presentation, National Renewable Energy Laboratory, 2014, https://research-hub.nrel.gov/en/publications/traction-drive-inverter-cooling-with-submerged-liquid-jet-impinge/.

[51]Narumanchi, "Light-Weight, Single-Phase, Liquid-Cooled Cold Plate."

[52]Zuckerman and Lior, "Jet Impingement Heat Transfer," pp. 581–582.

[53]Florschuetz, Metzger, and Truman, "Jet Array Impingement with Crossflow."

[54]Rattner, "General Characterization of Jet Impingement Array Heat Sinks."

[55]"Cooling Device," U.S. Patent 8,413,712, International Business Machines Corporation, granted 9 April 2013, https://patents.google.com/patent/US8413712B2/en.

[56]Florschuetz, Metzger, and Truman, "Jet Array Impingement with Crossflow."

[57]Florschuetz, Metzger, and Truman, "Jet Array Impingement with Crossflow."

[58]Holger Martin, "Heat and Mass Transfer between Impinging Gas Jets and Solid Surfaces," *Advances in Heat Transfer* 13 (1977): 1–60.

[59]Tiwei Wei, "High Efficiency Polymer based Direct Multi-jet Impingement Cooling Solution for High Power Devices," arXiv:2310.11663, preprint submitted 18 October 2023, https://arxiv.org/abs/2310.11663.

[60]Florschuetz, Metzger, and Truman, "Jet Array Impingement with Crossflow."

[61]Aaron M. Huber and Raymond Viskanta, "Effect of Jet-Jet Spacing on Convective Heat Transfer to Confined, Impinging Arrays of Axisymmetric Air Jets," *International Journal of Heat and Mass Transfer* 37, no. 18 (1994): 2859–2869, https://doi.org/10.1016/0017-9310(94)90340-9.

[62]Huber and Viskanta, "Confined Impinging Array of Air Jets with Spent Air Exits."

[63]Wei, "Direct Multi-jet Impingement Cooling Solution."

[64]Zuckerman and Lior, "Jet Impingement Heat Transfer."

[65]Rattner, "General Characterization of Jet Impingement Array Heat Sinks."

[66]David Ryan Hobby, “Generalized Pressure Drop and Heat Transfer Correlations for Jet Impingement Cooling with Jet Adjacent Fluid Extraction,” PhD diss., Colorado State University, 2022, https://mountainscholar.org/handle/10217/235294.

[67]Hobby, “Generalized Pressure Drop and Heat Transfer Correlations.”

[68]Derived in this paper. The crossflow mass flow after m rows is m times the jet flow per row-pitch, and the channel area per jet is y × z. The jet area is π d^2/4. The ratio of mass fluxes is therefore m (π/4)(d/y)(d/z). Nu/Nu0 then follows from the simplified correlation with the constants in the text. Equal flow per jet and uniform one-direction drainage are assumed.

[69]Florschuetz, Metzger, and Truman, “Jet Array Impingement with Crossflow.”

[70]Zuckerman and Lior, “Jet Impingement Heat Transfer,” p. 582.

[71]Florschuetz, Metzger, and Truman, “Jet Array Impingement with Crossflow.”

[72]Huber and Viskanta, “Confined Impinging Array of Air Jets with Spent Air Exits.”

[73]Rattner, “General Characterization of Jet Impingement Array Heat Sinks.”

[74]Huber and Viskanta, “Confined Impinging Array of Air Jets with Spent Air Exits.”

[75]Aaron Morgan Huber, “Heat Transfer with Impinging Gaseous Jet Systems,” PhD diss., Purdue University, n.d., https://docs.lib.purdue.edu/dissertations/AAI9420845.

[76]Rattner, “General Characterization of Jet Impingement Array Heat Sinks.”

[77]Thomas Brunschwiler et al., “Direct Liquid Jet-Impingement Cooling with Micron-Sized Nozzle Array and Distributed Return Architecture,” in *2006 10th IEEE Intersociety Conference on Thermal and Thermomechanical Phenomena in Electronics Systems (ITherm)* (2006), 196–203.

[78]Rattner, “General Characterization of Jet Impingement Array Heat Sinks.”

[79]U.S. Patent 8,413,712.

[80]Huber and Viskanta, “Confined Impinging Array of Air Jets with Spent Air Exits.”

[81]Rattner, “General Characterization of Jet Impingement Array Heat Sinks.”

[82]Hobby et al., “Water Jet Impingement Array with Interspersed Fluid Extraction.”

[83]Hobby, “Generalized Pressure Drop and Heat Transfer Correlations.”

[84]Brunschwiler et al., “Direct Liquid Jet-Impingement Cooling.”

[85]Zuckerman and Lior, “Jet Impingement Heat Transfer,” p. 586.

[86]Collins et al., “Additively Manufactured Microchannel Heat Sinks.”

[87]“Using a Multi-Inlet/Outlet Manifold to Improve Heat Transfer and Flow Distribution of a Pin Fin Heat Sink,” *Journal of Electronic Packaging* 144, no. 3 (September 2022): 031017, https://doi.org/10.1115/1.4054461.

[88]Hobby et al., “Water Jet Impingement Array with Interspersed Fluid Extraction.”

[89]Wei, “Direct Multi-jet Impingement Cooling Solution.”

[90]Hobby, “Generalized Pressure Drop and Heat Transfer Correlations.”

[91]Derived in this paper from the densities in Table 6 and an assumed plate thickness of 3 mm. 8.92 × 10.8 = 96.3 g; 8.89 × 10.8 = 96.0 g; 2.70 × 10.8 = 29.2 g. The thickness is an illustration and is not a CF-JET dimension.

[92]Copper Development Association, “Introduction to Copper.”

[93]Hoang et al., “3-D Printed Impingement Pin Fin Cold Plate.”

[94]Copper Development Association, “Introduction to Copper.”

[95]Hoang et al., “3-D Printed Impingement Pin Fin Cold Plate.”

[96]Narumanchi, “Light-Weight, Single-Phase, Liquid-Cooled Cold Plate.”

[97]“Thermal Management System and Method for Electronic Equipment Mounted on Coldplates,” U.S. Patent 7,092,255, Raytheon Company, granted 15 August 2006, https://patents.google.com/patent/US7092255B2/en.

[98]U.S. Patent 7,092,255.

[99]Narumanchi, “Light-Weight, Single-Phase, Liquid-Cooled Cold Plate.”

[100]Copper Development Association, “Introduction to Copper.”

[101]Hoang et al., “3-D Printed Impingement Pin Fin Cold Plate.”

[102]Barua et al., “Comparative Analysis of Direct and Indirect Cooling.”

[103]Walsh, “Microjet Impingement Cooling.”

[104]Zuckerman and Lior, “Jet Impingement Heat Transfer,” p. 566.

[105]Barua et al., “Comparative Analysis of Direct and Indirect Cooling.”

[106]Tuckerman and Pease, “High-Performance Heat Sinking for VLSI.”

[107]Sung and Mudawar, “Hybrid Micro-Channel/Slot-Jet Module.”

[108]Derived in this paper. 1.5 kW × 0.02 K/W = 30 K. 0.02 K/W × 36 cm² = 0.72 K·cm²/W = 72 mm²·K/W. 1 ÷ (0.02 K/W × 0.0036 m²) = 13,889 W/m²·K.

[109]The Dow Chemical Company, *DOWTHERM SR-1 Heat Transfer Fluid: Engineering Specifications for Closed-Loop HVAC Systems*, vendor specification, n.d., https://www.deppmann.com/wp-content/uploads/2016/08/DowTherm-SR-1-Specification.pdf.

[110]Hoang et al., “3-D Printed Impingement Pin Fin Cold Plate.”

[111]Hoang et al., “3-D Printed Impingement Pin Fin Cold Plate.”

[112]Dow, *DOWTHERM SR-1 Specifications*.

[113]SOL Engineering Services, *CF-JET*, Rev Final 2.

[114]Collins et al., “Additively Manufactured Microchannel Heat Sinks.”

[115]Hoang et al., “3-D Printed Impingement Pin Fin Cold Plate.”

[116]Hobby et al., “Water Jet Impingement Array with Interspersed Fluid Extraction.”

[117]Wei, “Direct Multi-jet Impingement Cooling Solution.”

[118]Narumanchi, “Light-Weight, Single-Phase, Liquid-Cooled Cold Plate.”

[119]Hobby, “Generalized Pressure Drop and Heat Transfer Correlations.”

[120]Florschuetz, Metzger, and Truman, “Jet Array Impingement with Crossflow.”